

---

# Scaling-laws for Large Time-series Models

---

**Thomas D. P. Edwards**  
 Johns Hopkins University  
 tedwar42@jhu.edu

**James Alvey**  
 University of Amsterdam  
 j.b.g.alvey@uva.nl

**Justin Alsing**  
 Calda AI  
 Oskar Klein Centre  
 justin@calda.ai

**Nam H. Nguyen**  
 Capital One  
 nam.nguyen@capitalone.com

**Benjamin D. Wandelt**  
 Institut d’Astrophysique de Paris  
 CCA, Flatiron Institute  
 bwandelt@iap.fr

## Abstract

Scaling laws for large language models (LLMs) have provided useful guidance on how to train ever larger models for predictable performance gains. Time series forecasting shares a similar sequential structure to language, and is amenable to large-scale transformer architectures. Here we show that foundational decoder-only time series transformer models exhibit analogous scaling-behavior to LLMs, while architectural details (aspect ratio and number of heads) have a minimal effect over broad ranges. We assemble a large corpus of heterogenous time series data on which to train, and establish, for the first time, power-law scaling relations with respect to parameter count, dataset size, and training compute, spanning five orders of magnitude.

## 1 Introduction

Time-series forecasting is fundamental to decision-making and scientific inference across all domains involving time-ordered observations. In fact, making probabilistic forecasts given past data (whether explicitly or implicitly) arguably underpins every human decision [1–5]. In industrial and scientific settings, time-series forecasting has traditionally involved supervised training of either statistical models (e.g., ARIMA, GARCH, state-space models, and others; see [6, 7] for reviews), bespoke dynamical models based on domain-specific knowledge, or more recently deep-learning based approaches trained for a specific forecasting task (see [8] for a review). While these approaches have formed the bedrock of time-series analysis up until now, key challenges and limitations remain: statistical models often fail to describe and capture the latent processes underlying the data, hampering their predictive utility; developing specialized problem-specific models requires considerable investment in human time and resources; and supervised deep-learning approaches trained on a single dataset are typically only useful in the data-rich regime, and generalize poorly to other problems.

The emergence of large language (LLMs; [9–12]) and computer vision models [13–19] with zero-shot prediction capabilities has sparked a growing interest in developing foundation models for time-series — general purpose models for forecasting, pre-trained on a large and diverse corpus of time-series data, with the aim of achieving state-of-the-art zero-shot forecasting performance across many domain areas [20–34]. Large time-series models (LTMs) are already achieving zero-shot prediction capability that is similar to (and in some cases better than) baseline statistical or domain-specific models in many areas [20–28, 34].

Underpinning the resource investment and subsequent success of LLMs and large-scale computer vision models was the demonstration of neural scaling laws [18, 35–40]. The observed power-law scaling of test loss with model sizes, compute resources, and training set sizes, has provided a basis

for predicting the expected gains from different efforts, aiding the community in allocating resources appropriately to achieve breakthroughs in performance. The establishment of similarly favourable neural scaling laws for LTMs would serve as both a motivation and guide in the pursuit of foundation models for time-series forecasting.

**Contributions:** In this work, we establish for the first time neural scaling laws for large time-series models (LTMs), demonstrating that LTMs enjoy similar power-law scaling laws to language and computer vision. We train decoder-only transformer models (with architectures tailored to time-series forecasting; §3.1) on a large, diverse, and well-balanced dataset comprising around 8 billion data points across 30,211,687 individual time-series, drawn from 38 qualitatively distinct data sources from varied areas (see §2). We demonstrate power-law like scaling behavior of model performance with model size, compute, and dataset size (Fig. 1). For each scaling case-study, we show similar scaling behavior in three key measures of the model performance: the mean-square error (MSE) characterizing the accuracy of point (posterior mean) forecasts; the Continuous Ranked Probability Score (CRPS [41]) characterizing the fidelity of the probabilistic predictions (ie., coverage of the forecast posterior density); and the log-likelihood loss characterizing the Kullback-Leibler (KL) divergence between the model and data generative distributions.

**Summary of Results:** In Fig. 1 we show the scaling of model performance (MSE, CRPS and log-likelihood) with model size (top row), compute (middle row), and dataset size (bottom row). We observe power-law scaling in the log-likelihood across the full range of parameters tested, whereas the MSE and CRPS show broken power-law behavior. Parameters of the fitted power-law functions can be found in Tab. 2. In Fig. 3 we show that the model performance is only weakly sensitive to architecture details (aspect ratio, and the number of heads).

**Compute Requirements:** To produce the results in this paper requires  $\mathcal{O}(50 - 70)$  individual production runs. Apart from the 100M parameter run, these were all carried out on single A100 NVIDIA GPU instances, each taking between 1 and 3 days to complete. As such, overall, the work presented here required  $\mathcal{O}(150)$  GPU-days of compute. To host the full dataset, we also required a CPU RAM allocation of approximately 250 GB.

## 2 Data

The development of a foundation model for time-series forecasting is predicated on the availability of a sufficiently large, diverse, and well-balanced dataset to train on. We constructed a corpus of time-series data comprising around 8 billion data points drawn from 38 varied data sources (see Tab. 1). For the purpose of this study, our focus was to ensure our dataset is: large enough so that for our largest models ( $\sim 100M$  parameters) we are still operating in the approximately infinite data limit (as discussed in the original LLM scaling-law paper [35]); as diverse as possible given the practical limitations on publicly available data; and balanced, such that no individual dataset comprises more than roughly 15% of the total number of data points. Our resulting dataset is competitive with the state-of-the-art in terms of both diversity and size<sup>1</sup>, while covering a wide variety of sampling frequencies, record lengths, dynamic ranges, and underlying latent process phenomenology. In this study we focus exclusively on univariate time-series forecasting, and leave the study of scaling-laws for multivariate LTMs to future work.

The data sources used to construct our dataset are summarized as follows (see also Tabs. 1, 3–7):

**Monash:** The Monash repository [42] is an open-source collection of data from many sources. We exclude datasets that are too short (shorter than our context length of 256; see § 3.1), and removed individual time-series that we found to destabilise training (due to e.g., a combination of heavy-tailed behavior and a large fraction of missing data). The included Monash data is summarized in Tab. 3.

**Climate:** We include climate data from two sources: the National Oceanic and Atmospheric Administration (NOAA), and the fifth generation European Centre for Medium-Range Weather Forecasts atmospheric reanalysis of the global climate (ERA5). From these we select a variety of different observables and sampling frequencies, summarized in Tabs. 4–5.

---

<sup>1</sup>Note that where other state-of-the-art time-series datasets from recent studies are larger, this discrepancy is largely accounted for by either the use of synthetic data in those studies (which we do not include in this work), and/or the reduction in our total data point numbers due to re-balancing of our data to ensure it is not dominated by a single data source.

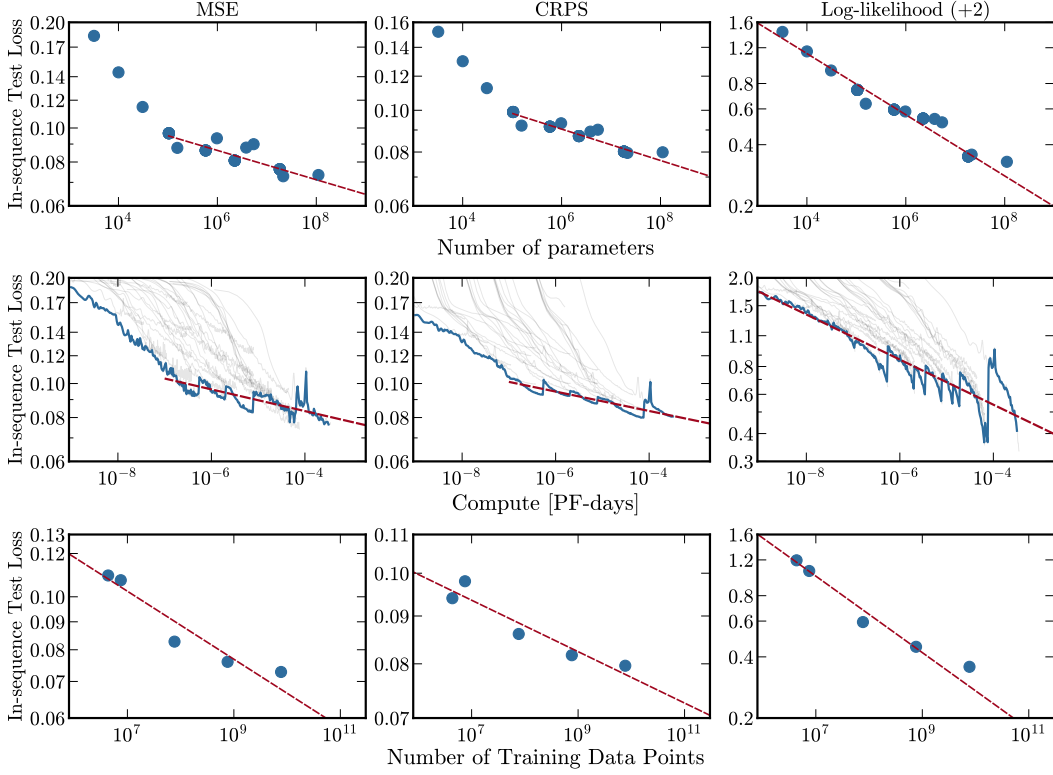


Figure 1: **Test Loss Scaling Laws:** Here we show three metrics for the minimum in-sequence test loss as a function of the number of parameters, compute, and dataset size. We demonstrate that, like language, the performance of large time-series models scales approximately as a power law with all three quantities. Note that we use the log-likelihood as the actual loss function for training. To ensure it remains positive for the power-law scaling we add a small constant.

**Energy:** Here we use a subset of the data from the BuildingsBench dataset [43]. The data is sampled at a fixed 15-minute cadence and represents energy demand across US commercial and real estate buildings.

**Traffic:** We use the LargeST [44] traffic dataset from 2017-2021 which represents traffic flow in California and is made up (once processed) of a total of 8520 series.

**Finance:** We source daily returns and trading volume data for 5038 stocks lists across various exchanges from yahoo finance (see Tab. 6). For trading volume, we model the logarithm of the data (due to the large dynamic range).

**Audio:** We include a diverse set of audio data from the *command*, *bird*, and *Arabic speech* datasets [45, 46]; see Tab. 7.

Each dataset is made up of a large number of individual time series of varying lengths. We use 95% of the set of time series for training and the remaining 5% for testing. Since the majority of the series are significantly longer than our context window, during training and testing we visit each series with probability  $p_i = t_i/T$ , where  $t_i$  is the number of data points in that series and  $T$  is the total number of data points in the training set. Additionally, each time we visit a series we choose a random starting index. This strategy ensures that the model sees each section of the data once (on average) in a given epoch. We normalize each time-series in the training set to have zero mean and unit standard deviation.<sup>2</sup>

<sup>2</sup>In rare instances where input time-series are constant (and hence have zero standard deviation), we set them to a constant value of zero.

Table 1: **Dataset summary.** M indicates million and B indicates billion.

	Monash	Climate	Energy	Traffic	Finance	Audio	Total
<b>Datasets</b>	23	15	2	5	2	3	38
<b># of data points</b>	503M	1.56B	2.5B	1.5B	42.6M	1.98B	8.13B
<b>% of data</b>	6.18%	19.19%	30.75%	18.45%	0.52%	24.35%	100%

### 3 Methods

#### 3.1 Model and Training Details

**Decoder-only Transformer:** We use decoder-only transformer models with self-attention as the primary architecture throughout, with a learned positional-encoding and flexible distribution head to make it more amenable to probabilistic time-series forecasting (as discussed below). We use a context length of 256 data points, and ReLU activation functions throughout.

**Learned Positional Encoding and Embedding:** Following the performance gains shown in Ref. [26], we use a learnable encoding rather than the sinusoidal positional encoding used in the original transformer model [47]. Both the learned positional encoding and embedding are simple linear layers going from one input to  $d_m$  outputs (see below). The positional encoding is treated in the usual fashion by just adding elementwise to the embedded float.

**Distribution Head:** The distribution head defines the distribution family modelled by the transformer, and is a critical architecture choice in enabling probabilistic forecasts with accurate coverage, as well as stable training and convergence. We use a Student’s- $t$  distribution head, where the mean,  $\mu$ , variance,  $\sigma^2$ , and degree of freedom,  $\nu$ , are separate outputs of the model.<sup>3</sup> The Student’s- $t$  distribution head allows us to model heavy-tailed data and processes, and in experiments we found that the Student’s- $t$  head enabled significantly more stable training than a Gaussian head (or simple posterior mean forecasting with an MSE loss). We note that in reality, many time-series data and underlying processes exhibit skewness, and a distribution head family that can describe asymmetric distributions would be well-motivated (e.g., Generalized gaussians, SinhArcSinh distributions, or more expressive normalizing flow or diffusion-based heads). We leave the exploration of more expressive distribution heads to future work.

We use a separate multi-layer perceptron (MLP) with four hidden layers of dimension  $d_m$  for each output of the distribution head, i.e., the mean, variance and degrees-of-freedom of the Student’s- $t$  distribution. In experiments we found that including separate MLPs for each distribution parameter (rather than a single MLP with three outputs), significantly stabilizes training. We use a negative log-likelihood loss throughout.

**Parameter Counting:** With this setup, the model architecture is defined by the following parameters: the number of output dimensions  $\theta_{\text{out}}$ , the input/output size of the linear layers in the self-attention  $d_m$ , the number of heads<sup>4</sup>  $N_{\text{heads}}$ , the hidden layer size of the linear layers directly after the self-attention  $d_{\text{ff}}$ , and the number of decoder layers  $N_l$ . Throughout this work we fix  $d_m = d_{\text{ff}}$  and treat all trainable parameters (including weights and biases of all layers) equally in the parameter counting. As shown in Fig. 1, we explore models with  $\sim 10^3$  to  $\sim 10^8$  trainable parameters.

**Training Details:** We use the AdamW optimizer with a batch size of 512, a cosine learning rate scheduler with a linear warm up of 3000 training steps, and train for a total of  $10^5$  steps. When training on the entire dataset ( $\sim 8$ B data points), this equates to roughly two epochs. To reduce computational costs we compute the test loss every  $\mathcal{O}(200)$  steps and average over a random 10% of the test data each time.

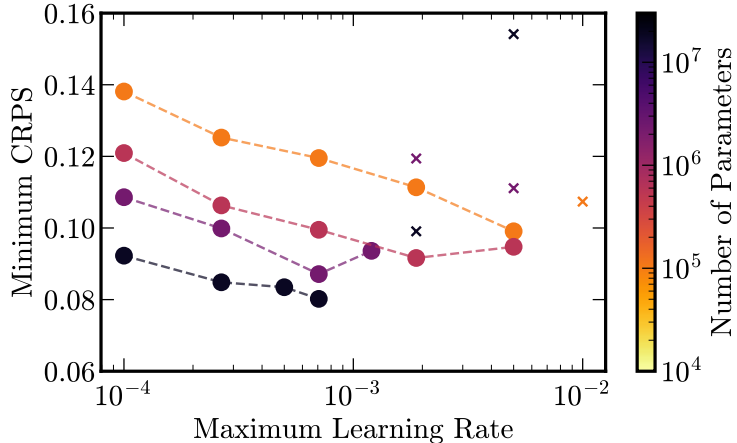


Figure 2: **Importance of Learning Rate:** Here we show the minimum CRPS measured on the test data as a function of the maximum learning rate reached at the end of the linear warm up schedule. Crosses indicate that the model diverged before training was complete. There is a clear optimum max learning rate which decreases as a function of model size/number of parameters.

### 3.2 Learning Rate and Architecture Dependence

In order to extract reliable scaling laws, we first need to determine the sensitivity of LTM performance as a function of both architecture choices (e.g., aspect ratio and number of heads), and learning rate scheduling.

**Learning Rate Scheduling:** In training we use a linear warm up followed by sinusoidal decay for the learning rate scheduling. In Fig. 2 we show the effect of changing the maximum learning rate reached at the end of the warm up. The performance of the model (CRPS) clearly depends on the maximum learning rate, and that dependence is itself a function of parameter count. The dependence on maximum learning rate is strong enough that it is possible to get better performance with a smaller model, if the maximum learning rate is too small (or too large) for the larger model. Moreover, for a fixed model size we see a clear optimum learning rate above which models diverge (shown as crosses on Fig. 2). To ensure that we used an optimal maximum learning rate as a function of model size, we fit a power law with a constant offset to the best models (at each parameter size) shown in Fig. 2. In the few cases for the largest models where our power law fit overestimates the optimal maximum learning rate (leading to divergence), we slowly reduce the learning rate until we achieve convergence.

**Aspect Ratio and Number of Heads:** Figure 3 shows how the minimum CRPS varies as a function of aspect ratio  $d_m/N_1$  (left panel) and the number of attention heads,  $N_{\text{heads}}$  (right panel). Overall, we find that neither of these choices have a large effect on performance; we note that this is similar to the weak architecture sensitivity observed for LLMs [35]. This is most clearly seen in the right panel of Fig. 3 where we are able to keep the number of parameters constant whilst varying the number of attention heads. For both model sizes tested, there is no significant change in the minimum CRPS achieved as more heads are added. For the main parameter, compute, and data scaling runs (the main results of this paper), we fix the number of heads to four.

Performance as a function of aspect ratio shows a slightly more complex behavior. In particular, we find smaller aspect ratios tend to perform better. However, this dependence is only weak up until aspect ratios of  $> 128$ , after which the model performance decreases substantially. Based on these observations, we keep the aspect ratio  $< 70$  for all scaling runs.

<sup>3</sup>We apply softplus activations to the distribution head outputs corresponding the variance and degrees-of-freedom, to ensure positive definiteness.

<sup>4</sup>Note that adding heads does not add to the parameter count. Instead the sequence is split and passed through different heads and recombined at the end. We therefore require that  $d_m \bmod N_{\text{heads}} = 0$

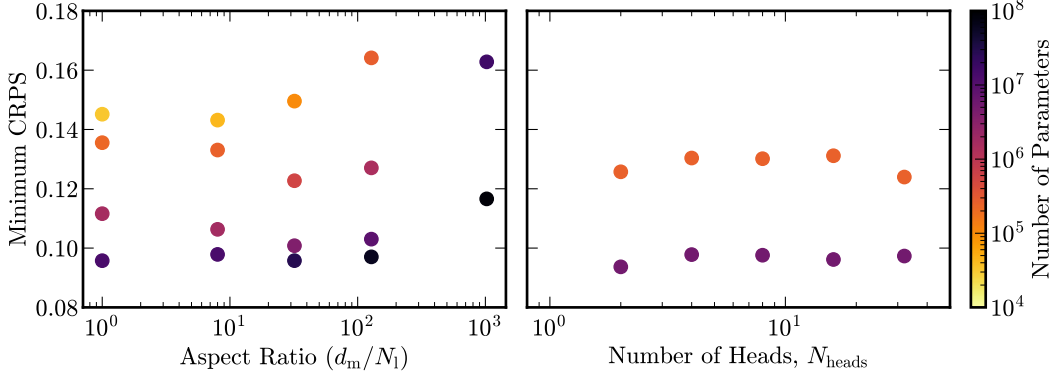


**Figure 3: Importance of Transformer Architecture:** We show the minimum CRPS on the test set as a function of architecture choices and number of parameters. *Left:* Performance on the test data has a weak dependence on aspect ratio below  $< 100$  but degrades significantly  $> 128$ . We therefore keep aspect ratios  $< 70$  for all scaling runs. *Right:* Here we see that the number of attention heads has no noticeable affect on the performance for both model sizes tested. We fix the number of heads to four for the scaling runs.

## 4 Scaling and Optimality

We now discuss the scaling results as a function of parameter count  $N_p$ , dataset size  $\mathcal{D}$ , and compute  $\mathcal{C}$ . For each scaling-relation, we fit a power law with the form:

$$L(A) = \left( \frac{A}{A_0} \right)^{-B_0}, \quad (1)$$

where  $L$  is the objective function (i.e., MSE, CRPS, or log-likelihood) and  $A$  is the quantity being scaled (i.e., parameter count  $N_p$ , dataset size  $\mathcal{D}$ , or compute  $\mathcal{C}$ ). The fitted values of the normalization  $A_0$  and index  $B_0$  for each scaling-law are given in Tab. 2. Where broken power-law like scaling is observed, we report the power law fit after the break only, since this is the relevant quantity to motivate extrapolation to larger models / datasets / compute resources.

### 4.1 Parameter Scaling

First we look at parameter scaling which is shown in the top panels of Fig. 1. In particular, we plot the in-sequence test loss computed for the MSE, CRPS, and log-likelihood (which is used as the loss function during training). For each model size we only plot the minimum test loss. We can see that all loss functions follow approximately power-law behavior over nearly five orders of magnitude in model size. This trend is particularly well observed in the log-likelihood. Note that we added a constant factor of two to the log-likelihood, to keep it positive.<sup>5</sup>

Interestingly, we do see a slight break in the power-law behavior in both the MSE and CRPS test losses, although this is mainly due to the behavior of models at very low parameter count. We plan to investigate the details of this break in future work. To ensure that power-law scaling isn't biased by this break, we only fit to models with  $> 10^5$  parameters. This difference between the MSE and log-likelihood is not surprising as the MSE only tests the performance of the model to predict the mean whereas the log-likelihood captures the distribution. On the other hand, the difference in the scaling behavior seen across the CRPS score is slightly more surprising. A possible explanation for this discrepancy is that the log-likelihood is known to be more sensitive to variations in the tails of the forecast (Student's- $t$ ) distribution [48]. Regardless of these details, this observed scaling over many orders of magnitude is remarkable and demonstrates that LTM are likely to reach state-of-the-art performance given enough data and model size.

<sup>5</sup>We note here that a constant additive factor can change the slope of the fitted power-law. To remain as agnostic as possible we choose to add the smallest integer required to make all values of the loss positive (i.e., two).

Table 2: **Power-law fits.**

	MSE		CRPS		Log-Likelihood	
	$\log_{10}(A_0)$	$B_0$	$\log_{10}(A_0)$	$B_0$	$\log_{10}(A_0)$	$B_0$
Number of Parameters, $N_p$	-19.47	0.042	-22.64	0.036	4.33	0.151
Training Compute, $\mathcal{C}$	-38.88	0.031	-43.03	0.028	-6.65	0.101
Dataset Size, $\mathcal{D}$	-8.91	0.062	-30.42	0.027	7.00	0.188

## 4.2 Data Scaling

Scaling the dataset in a coherent manner requires some care. In particular, we find that to achieve reliable scaling behavior as the dataset size grows requires one to keep the diversity approximately fixed i.e., the proportion of each dataset’s contribution to the total must remain the same (see Tab. 1). For data that is significantly longer than our context length, we simply use a random fraction,  $f_d$ , of each time series. For data that would become shorter than our context length once cut, we instead randomly drop the entire series with probability equal to  $1 - f_d$ . To compute the test loss, however, we average over the full test set as in the parameter scaling runs. This is to allow direct comparison between data scaling runs with different values of  $f_d$ , and reduce the noise in the test loss computation for small dataset sizes.

Results are shown in the bottom panel of Fig. 1 where we train a  $\sim 20M$  parameter model using the optimum max learning rate found during the parameter scaling exploration as well as early stopping. We again find power-law scaling across approximately four orders of magnitude. Interestingly, all three loss functions scale as a power law over the full range tested, although there is a mild indication of saturation for the largest dataset sizes.<sup>6</sup> Results of the power-law fits are shown in the bottom row of Tab. 2.

## 4.3 Compute Scaling

Finally, we turn to compute scaling where we again follow a similar method to Ref. [35]. In particular, the compute at any given stage in the training process is given by  $\mathcal{C} = 6BN_pL_{\text{seq}}$  where  $B$  is the batch size,  $N_p$  is the number of parameters in the model, and  $L_{\text{seq}}$  is the context length. Test losses as a function of compute are shown in Fig. 1 (middle panel) and the scaling law is obtained by taking the minimum value at any given value of compute. Although we see a significant amount of noise in the loss functions during training, there is a clear overall trend towards lower test losses for higher compute which is accurately tracked by a power law.

Similarly to the parameter scaling we see a slight break at low values of compute for both the MSE and CRPS test losses. We therefore again choose to only fit to data above  $10^{-7}$  PF-days. Finally, we note that the steepness of the log-likelihood test losses at large compute values indicates that the models are not yet fully converged. The effect is more dramatic at larger model sizes, indicating that further tuning of the models and learning rate scheduling can still improve performance. We empirically observe that the test loss tends to plateau in the middle of training and then decrease again as the scheduler reaches low values of the learning rate (towards the end of the sinusoidal decay). Further work is needed to test whether an alternative scheduler can improve overall performance and thus further improve model scaling.

## 5 Discussion and Limitations

Throughout this paper we have focused on evaluating models by their in-sequence test loss, and have not discussed explicitly how this translates into a model’s ability to forecast into the future. Again taking inspiration from LLMs, we have implicitly assumed that a model which produces good in-sequence predictions should naturally be able to forecast into the future. This is theoretically and empirically well-motivated; as the modelled posterior predictive distribution for the next value

<sup>6</sup>Ideally we would use a larger model to ensure we are operating in the approximately infinite parameter limit, but we were limited by computational resources.

becomes increasingly well-calibrated, any accumulating errors from auto-regressively rolling out those predictions into the future should also decrease (leading to more accurate prediction further into the future). In App. B, we show some clear examples of how forecast roll-out becomes increasingly coherent with increasing model size (and corresponding decreases in test loss) [25, 34]. We leave the study of scaling-laws based on rolled out forecasting ability (on different time horizons) to future work.

We have detailed the specific scaling laws for a decoder-only transformer with self-attention. However, it would be interesting to explore how modifications to this architecture might improve model scaling. In particular, much of the recent progress in using LTMs [20–28, 34] has involved various changes to transformer architectures to make them more suited to time-series data. We advocate for comparative scaling law studies as new architectures are introduced, to allow the community to evaluate which model architectures will eventually reach state-of-the-art zero-shot prediction capabilities.

When experimenting with data scaling, we found it was necessary to scale the training data in such a way as to (approximately) preserve the data diversity in the scaled training set (i.e., keep relative contributions of each data source constant). Approaches to data scaling that did not preserve data diversity failed to reveal clear scaling behaviour; we attributed this to the resulting variation in data diversity dominating over any scaling behaviour. Given the importance of training data diversity in establishing data scaling laws, and in training state-of-the-art pre-trained foundation models in general, developing a robust framework for measuring data diversity would be of great utility to the field. Taking inspiration from Ref. [49], one avenue could be looking at the impact of new data sources on gradients during training; data which produce gradients with a high cosine similarity compared to the current training set would be likely to increase data diversity. We leave exploration of measures of data diversity to future work.

An additional scaling law that we have not explored in this work (due to computational limitations) is performance as a function of increasing context length. Multiple studies (e.g., [34, 50]), both for LLMs and LTMs, have shown that increasing the context length window significantly improves both in-sequence prediction as well as forecasting. This should be particularly apparent for time series data as increasing context length gives the LTMs access to lower frequency modes of variability, which might otherwise be missed. We will explore context-length scaling in future work.

In this work we have focused exclusively on univariate time-series data. However, a general purpose foundation model for time-series forecasting should be able to cope with the more general setting of multivariate time-series prediction, while accounting for multiple exogenous covariates. Establishing scaling-laws for multivariate time-series forecasting would be an important extension to this work. This will demand the assembly of a large and diverse training set of multivariate data, each with their own (varying number of) exogenous factors.

Finally, the literature on transformers for time series forecasting has, to date, mostly focused on trying to achieve state-of-the-art performance on a small set of benchmark experiments. Our results indicate that large scale pre-training leads to scalable performance improvements that, given enough time and compute, can result in state-of-the-art performance across the majority of benchmarks.

**Impact Statement and Ethics:** The main goal of this paper is to advance the fields of machine learning and foundational time series forecasting. Time series forecasting has numerous applications across both commercial sectors and other critical areas such as healthcare, climate science, finance, and energy management. By improving forecasting techniques, our work can contribute to more accurate predictions and better decision-making in these diverse fields. Due the exploratory nature of this work, it is highly unlikely that there are direct negative societal impacts of the current study. In addition, there are no specific ethical implications of our work that are relevant for further discussion here. Indeed, we confirm that everything in this paper complies with the NeurIPS Code of Ethics.

**Acknowledgments:** TE thanks Jared Kaplan for providing initial motivation that these scaling laws would appear. TE is supported by the Horizon Postdoctoral Fellowship. We thank Hiranya Peiris for providing access to GPU compute resources. JA has been supported by funding from the European Research Council (ERC) under the European Union’s Horizon 2020 research and innovation programmes (grant agreement no. 101018897 CosmicExplorer). This work partly was carried out at the Advanced Research Computing at Hopkins (ARCH) core facility (rockfish.jhu.edu), which is supported by the National Science Foundation (NSF) grant number OAC 1920103. Some of this work was also carried out on the Snellius Compute Cluster at SURFsara.

## References

- [1] K. P. Kording and D. M. Wolpert, “Bayesian integration in sensorimotor learning,” *Nature*, vol. 427, no. 6971, pp. 244–247, 2004.
- [2] K. Doya, *Bayesian brain: Probabilistic approaches to neural coding*. MIT press, 2007.
- [3] K. Doya, “Modulators of decision making,” *Nature neuroscience*, vol. 11, no. 4, pp. 410–416, 2008.
- [4] A. Funamizu, B. Kuhn, and K. Doya, “Neural substrate of dynamic bayesian inference in the cerebral cortex,” *Nature neuroscience*, vol. 19, no. 12, pp. 1682–1689, 2016.
- [5] C. Lindig-León, N. Kaur, and D. A. Braun, “From bayes-optimal to heuristic decision-making in a two-alternative forced choice task with an information-theoretic bounded rationality model,” *Frontiers in Neuroscience*, vol. 16, p. 906198, 2022.
- [6] M. West and J. Harrison, *Bayesian Forecasting and Dynamic Models*. Springer Series in Statistics, Springer New York, 2013.
- [7] R. J. Hyndman and G. Athanasopoulos, *Forecasting: principles and practice*. OTexts, 2018.
- [8] J. F. Torres, D. Hadjout, A. Sebaa, F. Martínez-Álvarez, and A. Troncoso, “Deep learning for time series forecasting: a survey,” *Big Data*, vol. 9, no. 1, pp. 3–21, 2021.
- [9] J. Devlin, M.-W. Chang, K. Lee, and K. Toutanova, “Bert: Pre-training of deep bidirectional transformers for language understanding,” *arXiv preprint arXiv:1810.04805*, 2018.
- [10] T. Brown, B. Mann, N. Ryder, M. Subbiah, J. D. Kaplan, P. Dhariwal, A. Neelakantan, P. Shyam, G. Sastry, A. Askell, *et al.*, “Language models are few-shot learners,” *Advances in neural information processing systems*, vol. 33, pp. 1877–1901, 2020.
- [11] H. Touvron, L. Martin, K. Stone, P. Albert, A. Almahairi, Y. Babaei, N. Bashlykov, S. Batra, P. Bhargava, S. Bhosale, *et al.*, “Llama 2: Open foundation and fine-tuned chat models,” *arXiv preprint arXiv:2307.09288*, 2023.
- [12] H. W. Chung, L. Hou, S. Longpre, B. Zoph, Y. Tay, W. Fedus, Y. Li, X. Wang, M. Dehghani, S. Brahma, *et al.*, “Scaling instruction-finetuned language models,” *Journal of Machine Learning Research*, vol. 25, no. 70, pp. 1–53, 2024.
- [13] A. Dosovitskiy, L. Beyer, A. Kolesnikov, D. Weissenborn, X. Zhai, T. Unterthiner, M. Dehghani, M. Minderer, G. Heigold, S. Gelly, *et al.*, “An image is worth 16x16 words: Transformers for image recognition at scale,” *arXiv preprint arXiv:2010.11929*, 2020.
- [14] A. Radford, J. W. Kim, C. Hallacy, A. Ramesh, G. Goh, S. Agarwal, G. Sastry, A. Askell, P. Mishkin, J. Clark, *et al.*, “Learning transferable visual models from natural language supervision,” in *International conference on machine learning*, pp. 8748–8763, PMLR, 2021.
- [15] A. Ramesh, M. Pavlov, G. Goh, S. Gray, C. Voss, A. Radford, M. Chen, and I. Sutskever, “Zero-shot text-to-image generation,” in *International conference on machine learning*, pp. 8821–8831, Pmlr, 2021.
- [16] W. Yan, Y. Zhang, P. Abbeel, and A. Srinivas, “Videogpt: Video generation using vq-vae and transformers,” *arXiv preprint arXiv:2104.10157*, 2021.
- [17] A. Arnab, M. Dehghani, G. Heigold, C. Sun, M. Lučić, and C. Schmid, “Vivit: A video vision transformer,” in *Proceedings of the IEEE/CVF international conference on computer vision*, pp. 6836–6846, 2021.
- [18] K. He, X. Chen, S. Xie, Y. Li, P. Dollár, and R. Girshick, “Masked autoencoders are scalable vision learners,” in *Proceedings of the IEEE/CVF conference on computer vision and pattern recognition*, pp. 16000–16009, 2022.

[19] J. Li, D. Li, S. Savarese, and S. Hoi, “Blip-2: Bootstrapping language-image pre-training with frozen image encoders and large language models,” in *International conference on machine learning*, pp. 19730–19742, PMLR, 2023.

[20] A. Das, W. Kong, R. Sen, and Y. Zhou, “A decoder-only foundation model for time-series forecasting,” *arXiv e-prints*, p. arXiv:2310.10688, Oct. 2023.

[21] M. Goswami, K. Szafer, A. Choudhry, Y. Cai, S. Li, and A. Dubrawski, “MOMENT: A Family of Open Time-series Foundation Models,” *arXiv e-prints*, p. arXiv:2402.03885, Feb. 2024.

[22] K. Rasul, A. Ashok, A. R. Williams, A. Khorasani, G. Adamopoulos, R. Bhagwatkar, M. Biloš, H. Ghonia, N. V. Hassen, A. Schneider, S. Garg, A. Drouin, N. Chapados, Y. Nevmyvaka, and I. Rish, “Lag-Llama: Towards Foundation Models for Time Series Forecasting,” *arXiv e-prints*, p. arXiv:2310.08278, Oct. 2023.

[23] A. Garza and M. Mergenthaler-Canseco, “TimeGPT-1,” *arXiv e-prints*, p. arXiv:2310.03589, Oct. 2023.

[24] Y. Nie, N. H. Nguyen, P. Sinthong, and J. Kalagnanam, “A Time Series is Worth 64 Words: Long-term Forecasting with Transformers,” *arXiv e-prints*, p. arXiv:2211.14730, Nov. 2022.

[25] G. Woo, C. Liu, A. Kumar, C. Xiong, S. Savarese, and D. Sahoo, “Unified Training of Universal Time Series Forecasting Transformers,” *arXiv e-prints*, p. arXiv:2402.02592, Feb. 2024.

[26] G. Woo, C. Liu, A. Kumar, and D. Sahoo, “Pushing the Limits of Pre-training for Time Series Forecasting in the CloudOps Domain,” *arXiv e-prints*, p. arXiv:2310.05063, Oct. 2023.

[27] W. Xue, T. Zhou, Q. Wen, J. Gao, B. Ding, and R. Jin, “CARD: Channel Aligned Robust Blend Transformer for Time Series Forecasting,” *arXiv e-prints*, p. arXiv:2305.12095, May 2023.

[28] R. Ilbert, A. Odonnat, V. Feofanov, A. Virmaux, G. Paolo, T. Palpanas, and I. Redko, “Unlocking the Potential of Transformers in Time Series Forecasting with Sharpness-Aware Minimization and Channel-Wise Attention,” *arXiv e-prints*, p. arXiv:2402.10198, Feb. 2024.

[29] D. Salinas, V. Flunkert, J. Gasthaus, and T. Januschowski, “Deepar: Probabilistic forecasting with autoregressive recurrent networks,” *International journal of forecasting*, vol. 36, no. 3, pp. 1181–1191, 2020.

[30] B. N. Oreshkin, D. Carpow, N. Chapados, and Y. Bengio, “N-beats: Neural basis expansion analysis for interpretable time series forecasting,” *arXiv preprint arXiv:1905.10437*, 2019.

[31] B. N. Oreshkin, D. Carpow, N. Chapados, and Y. Bengio, “Meta-learning framework with applications to zero-shot time-series forecasting,” in *Proceedings of the AAAI Conference on Artificial Intelligence*, vol. 35, pp. 9242–9250, 2021.

[32] N. Gruver, M. Finzi, S. Qiu, and A. G. Wilson, “Large language models are zero-shot time series forecasters,” *Advances in Neural Information Processing Systems*, vol. 36, 2024.

[33] Q. Ma, Z. Liu, Z. Zheng, Z. Huang, S. Zhu, Z. Yu, and J. T. Kwok, “A survey on time-series pre-trained models,” *arXiv preprint arXiv:2305.10716*, 2023.

[34] A. Fatir Ansari, L. Stella, C. Turkmen, X. Zhang, P. Mercado, H. Shen, O. Shchur, S. Sundar Rangapuram, S. Pineda Arango, S. Kapoor, J. Zschiegner, D. C. Maddix, H. Wang, M. W. Mahoney, K. Torkkola, A. G. Wilson, M. Bohlke-Schneider, and Y. Wang, “Chronos: Learning the Language of Time Series,” *arXiv e-prints*, p. arXiv:2403.07815, Mar. 2024.

[35] J. Kaplan, S. McCandlish, T. Henighan, T. B. Brown, B. Chess, R. Child, S. Gray, A. Radford, J. Wu, and D. Amodei, “Scaling Laws for Neural Language Models,” *arXiv e-prints*, p. arXiv:2001.08361, Jan. 2020.

[36] M. Tan and Q. Le, “Efficientnet: Rethinking model scaling for convolutional neural networks,” in *International conference on machine learning*, pp. 6105–6114, PMLR, 2019.

[37] M. Tan and Q. Le, “Efficientnetv2: Smaller models and faster training,” in *International conference on machine learning*, pp. 10096–10106, PMLR, 2021.

[38] M. Raghu, T. Unterthiner, S. Kornblith, C. Zhang, and A. Dosovitskiy, “Do vision transformers see like convolutional neural networks?,” *Advances in neural information processing systems*, vol. 34, pp. 12116–12128, 2021.

[39] C. Riquelme, J. Puigcerver, B. Mustafa, M. Neumann, R. Jenatton, A. Susano Pinto, D. Keysers, and N. Houlsby, “Scaling vision with sparse mixture of experts,” *Advances in Neural Information Processing Systems*, vol. 34, pp. 8583–8595, 2021.

[40] T. Henighan, J. Kaplan, M. Katz, M. Chen, C. Hesse, J. Jackson, H. Jun, T. B. Brown, P. Dhariwal, S. Gray, *et al.*, “Scaling laws for autoregressive generative modeling,” *arXiv preprint arXiv:2010.14701*, 2020.

[41] H. Hersbach, “Decomposition of the continuous ranked probability score for ensemble prediction systems,” *Weather and Forecasting*, vol. 15, no. 5, pp. 559–570, 2000.

[42] R. Godahewa, C. Bergmeir, G. I. Webb, R. J. Hyndman, and P. Montero-Manso, “Monash time series forecasting archive,” in *Neural Information Processing Systems Track on Datasets and Benchmarks*, 2021.

[43] P. Emami, A. Sahu, and P. Graf, “Buildingsbench: A large-scale dataset of 900k buildings and benchmark for short-term load forecasting,” *Advances in Neural Information Processing Systems*, 2023.

[44] X. Liu, Y. Xia, Y. Liang, J. Hu, Y. Wang, L. Bai, C. Huang, Z. Liu, B. Hooi, and R. Zimmermann, “Largest: A benchmark dataset for large-scale traffic forecasting,” in *Advances in Neural Information Processing Systems*, 2023.

[45] P. Warden, “Speech Commands: A Dataset for Limited-Vocabulary Speech Recognition,” *arXiv e-prints*, p. arXiv:1804.03209, Apr. 2018.

[46] D. Stowell, M. D. Wood, H. Pamuła, Y. Stylianou, and H. Glotin, “Automatic acoustic detection of birds through deep learning: The first bird audio detection challenge,” *Methods in Ecology and Evolution*, vol. 10, no. 3, pp. 368–380, 2019.

[47] A. Vaswani, N. Shazeer, N. Parmar, J. Uszkoreit, L. Jones, A. N. Gomez, Ł. Kaiser, and I. Polosukhin, “Attention is all you need,” *Advances in neural information processing systems*, vol. 30, 2017.

[48] M. B. Bjerrregård, J. K. Møller, and H. Madsen, “An introduction to multivariate probabilistic forecast evaluation,” *Energy and AI*, vol. 4, p. 100058, 2021.

[49] S. McCandlish, J. Kaplan, D. Amodei, and OpenAI Dota Team, “An Empirical Model of Large-Batch Training,” *arXiv e-prints*, p. arXiv:1812.06162, Dec. 2018.

[50] Gemini Team, “Gemini 1.5: Unlocking multimodal understanding across millions of tokens of context,” *arXiv e-prints*, p. arXiv:2403.05530, Mar. 2024.

[51] R. Lam, A. Sanchez-Gonzalez, M. Willson, P. Wirnsberger, M. Fortunato, F. Alet, S. Ravuri, T. Ewalds, Z. Eaton-Rosen, W. Hu, A. Merose, S. Hoyer, G. Holland, O. Vinyals, J. Stott, A. Pritzel, S. Mohamed, and P. Battaglia, “Learning skillful medium-range global weather forecasting,” *Science*, vol. 382, pp. 1416–1421, Dec. 2023.

[52] J. Pathak, S. Subramanian, P. Harrington, S. Raja, A. Chattopadhyay, M. Mardani, T. Kurth, D. Hall, Z. Li, K. Azizzadenesheli, P. Hassanzadeh, K. Kashinath, and A. Anandkumar, “Four-CastNet: A Global Data-driven High-resolution Weather Model using Adaptive Fourier Neural Operators,” *arXiv e-prints*, p. arXiv:2202.11214, Feb. 2022.

[53] E. J. H. Wilson, A. Parker, A. Fontanini, E. Present, J. L. Reyna, R. Adhikari, C. Bianchi, C. CaraDonna, M. Dahlhausen, J. Kim, A. LeBar, L. Liu, M. Praprost, L. Zhang, P. DeWitt, N. Merket, A. Speake, T. Hong, H. Li, N. M. Frick, Z. Wang, A. Blair, H. Horsey, D. Roberts, K. Trenbath, O. Adekanye, E. Bonnema, R. El Kontar, J. Gonzalez, S. Horowitz, D. Jones, R. T. Muehleisen, S. Platthotam, M. Reynolds, J. Robertson, K. Sayers, and Q. Li, “End-use load profiles for the u.s. building stock: Methodology and results of model calibration, validation, and uncertainty quantification,” *Technical Report*, 3 2022.

## A Dataset Details

In this section we detail the various sources that form the basis of our dataset and the choices made during its construction. Throughout data acquisition we had two critical features that the dataset needed to satisfy to facilitate the study of the main paper. Firstly, we needed a large enough dataset to train models up to  $\mathcal{O}(100)M$  parameters. This is particularly important as the original work [35] demonstrated scaling laws over many orders of magnitude. Although we were limited here by computational resources, it was important to explore the parameter range  $10^3 - 10^8$  (the current range used in other transformer based time series models). Secondly, the dataset needed to be sufficiently balanced across sources and features such that the scaling laws observed here can be considered a feature of foundation models and not associated with a particular dataset.

Taking inspiration from large language models [35], we therefore aimed to gather around  $\mathcal{O}(10^{10})$  data points from a variety of domains. We note, however, that treating a single floating point number on a similar footing to a language token is not necessarily a good comparison. In particular, language tokens can contain significantly more semantic meaning than a floating point number can. It's therefore likely that we will need more data points overall, although more work is required to make this comparison more precise. Before detailing our particular sources, we would like to emphasize that there is an enormous corpus of time series data publicly available but is not currently formatted for easy downloading and processing. Ref. [25] is the first paper to open-source a fairly large dataset but significant work is still required to expand its size and diversity.<sup>7</sup> For example, large-scale, state-of-the-art language models are likely trained on well over a trillion tokens.

We now discuss each dataset presented in Tab. 1. Overall, we assembled approximately 8B data points from six domains, each with a its own source of variation.

All data used throughout this work has been labelled/licensed as free to use for non-commercial purposes with the appropriate citations. We have included the appropriate citations where necessary below.

### A.1 Monash

The Monash dataset has been the default repository of open-source time series data used by the academic community for some time [42]. It contains data from a huge variety of sources and contains a wide variety of characteristics. For this work we exclude series that are either too short or are particularly noisy.<sup>8</sup> We are then left with a total of 23 different sources which add up to a total of  $\sim 500M$  data points; details are given in Tab. 3.

### A.2 Climate

Our climate dataset, made up of around 1.5B data points, has two primary sources: the National Oceanic and Atmospheric Administration (NOAA) and the fifth generation European Centre for Medium-Range Weather Forecasts atmospheric reanalysis of the global climate (ERA5). Each source provides approximately 750M data points split across a variety of observables and time frames.

We note here that since the global climate is a correlated system, forecasting a single variable into the future whilst ignoring the evolution of the rest of the system is intrinsically difficult (maybe impossible in some cases). Nevertheless, each time series can provide important information from which the foundation model can learn correlations. Moreover, some seasonal trends are very stable and predictable from a single time series. Future work should carefully consider how to include climate data in a way that allows the model to exploit correlations inherent in the data [51, 52].

**NOAA:** We primarily gather data from NOAA high-resolution blended analysis of daily sea surface temperature (SST) which includes both temperature measurements and ice level measurements on a  $0.25^\circ$  grid worldwide.<sup>9</sup> Weather at different points of the grid are intrinsically correlated, especially

---

<sup>7</sup>Note that by the time this data became open-source we had already fixed our dataset.

<sup>8</sup>We found through experimentation that removing very noisy datasets significantly improved training stability.

<sup>9</sup>The original data can be found here <https://downloads.psl.noaa.gov/Datasets/noaa.oisst.v2.highres/>.

Table 3: **Monash Data:** For each dataset we list the sampling frequency, the total number of series, and the total number of data points.

Dataset	Frequency	Number of Series	Number of Data Points
London Smart Meters	Half Hourly	5,560	166.5M
Wind Farms	Every Minute	339	172.1M
Wind Power	4 Seconds Intervals	1	7.4M
Solar Power	4 Second Intervals	1	7.4M
Oikolab Weather	Hourly	8	0.8M
Elecemand	Half Hourly	1	17.5k
Kaggle Web Traffic	Daily	145,063	116.5M
Tourism Quarterly	Quarterly	427	42.5k
Tourism Monthly	Monthly	366	109.3k
CIF 2016	Monthly	72	7.1k
Traffic Weekly	Weekly	862	89.6k
Traffic Hourly	Hourly	862	15.1M
Australian Electricity	Half Hourly	5	1.2M
Sunspot	Daily	1	73.9k
Hospital	Monthly	767	64.4k
NN5 Daily	Daily	111	87.8k
NN5 Weekly	Weekly	111	12.5k
M4 Hourly	Hourly	414	373.4k
Fred MD	Monthly	107	77.9k
Solar Weekly	Weekly	137	7.1k
Solar 10 Minutes	10 Minute Intervals	137	7.2M
Electricity Weekly	Weekly	321	50.1k
Electricity Hourly	Hourly	321	8.4M

Table 4: **NOAA Data:** For each dataset we list the sampling frequency, the total number of series, the length of each series, and the total number of data points.

Dataset	Frequency	Number of Series	Length	Number of Data Points
SST Mean	Daily	582241	365	212.5M
SST Anomalies	Daily	581249	365	212.1M
SST Long Term Average	Daily	218211	365	79.6M
SST Monthly Average	Monthly	72730	509	37M
SST Weekly Average	Monthly	72689	2214	161M
Ice Mean	Daily	63971	365	23M
Ice Long Term Average	Daily	12451	365	4.5M
Ice Monthly Average	Daily	5363	509	2.7M
Radiation Long Term Average	Daily	6622	365	2.4M

on such small grid sizes. We therefore downsample the data by a factor of three by randomly choosing grid points without replacement (we do this independently for each dataset).

To ensure we have data that covers a wide range of time scales and variability we pick a variety of observables shown in Tab. 4. For the daily data we pick 8 years of data, each separated by 5 years

(spread out to maximize data diversity i.e., minimize year to year correlations) but skip leap years for easier data processing (so all arrays are 365 elements long). The final year selection is 1985, 1990, 1995, 2001, 2005, 2010, 2015, and 2021. This size of this dataset could easily be supplemented simply by adding more of the 40 years of available data.

For additional diversity we use the same method to extract outgoing long wave radiation time series from [https://downloads.psl.noaa.gov/Datasets/uninterp\\_OLR/](https://downloads.psl.noaa.gov/Datasets/uninterp_OLR/). This is the shown in the final row of Tab. 4.

Table 5: **ERA5 Data:** Similar to above. The different number of series for each dataset is due to the randomness in the subsampling.

Dataset	Frequency	Number of Series	Length	Number of Data Points
Sea Level Pressure	4 Hour Intervals	63094	2190	138M
2m Temp.	4 Hour Intervals	63190	2190	138M
2m Dewpoint Temp.	4 Hour Intervals	63123	2190	138M
Surface Pressure	4 Hour Intervals	63263	2190	139M
10m V Wind Comp.	4 Hour Intervals	63263	2190	139M
10m U Wind Comp.	4 Hour Intervals	63220	2190	138M

**ERA5:** We take a similar approach to above when processing/gathering ERA5 data. Here though, we focus on higher frequencies by using a single year of data (2001) sampled every four hours. We additionally use different data variables (the six most popular variables) to ensure that the data features are likely different to those present in the NOAA data. ERA5 data is also originally on a  $0.25^\circ$  global grid which we randomly down sample by a factor of four. Details are given in Tab. 5.

### A.3 Energy

For the energy dataset, we use the benchmark dataset prepared in the `BuildingsBench` data release [43]. In particular, we choose to sample 2.5B data points from the full dataset (which totals over 15B individual data points). These 2.5B data points, which overall constitute approximately 30% of our full dataset, are all taken from the Buildings-900K database. These time series represent a large-scale sample of simulated US building energy demand and are designed to be broadly representative of US commercial and residential building stock. As described in [43], the dataset is originally sourced from the NREL EULP database [53], which provides 15- minute resolution, appliance-level consumption for 550K residential and 350K commercial buildings spread across all climate regions in the U.S. For more finer-grained details, see App. B.3 in Ref. [43].

### A.4 Traffic

We consider the public LargeST [44] dataset which is a collection of 8600 time series recorded from traffic sensors in the California area. The data spans over 5 years, from 2017 to 2021, and is sampled at 15 minute resolution. To reduce the data size, we down-sample the data to hourly resolution and remove series that contains over 50% missing entries. This gives us a total of 8520 series all with length 175296, which translates to 1.46B data points.

### A.5 Finance

We include daily stock returns and volume data, treated as separate one-dimensional time-series respectively, for 5038 stocks listed across the Nasdaq, NYSE, and AMEX stock exchanges. Daily stock returns and volume tickers are obtained for 7230 stocks from `yahoo finance`, from the beginning of each listing up to 1st January 2024. We discard any stocks that have fewer than 512 ticks (recorded trading days), and any series containing NaN or inf. This results in time-series for 5038 stocks, with both returns and volume data, and a total of 42.6M data points (Tab. 6).

Table 6: **Finance Data:** Daily stock returns and volume data for 5038 stocks listed across the Nasdaq, NYSE and AMEX exchanges, obtained from yahoo finance.

Dataset	Frequency	Number of Series	Number of Data Points
Stock Returns	Daily	5038	26.3M
Stock Volume	Daily	5038	26.3M

## A.6 Audio

Audio data is intrinsically a one dimensional time series rich with structure and features; it is therefore perfectly suited for our study. We have three primary sources of audio data, all from the DagsHub Open-Source Audio Datasets repository (<https://github.com/DagsHub/audio-datasets>). Again, the total volume of data here is extremely large and can be used to supplement future datasets for larger models. Here we use three particular sources each from a different domain to enhance its diversity. As presented in Tab 1, these three sources add up to approximately 2B data points and  $\sim 25\%$  of our overall dataset. A summary of the three sources can be found in Tab. 7

Table 7: **Audio Data:** Similar to above.

Dataset	Frequency	Number of Series	Length	Number of Data Points
Commands	16 kHz	47650	16,000	762.4M
Arabic Speech	24 kHz	1813	Varied	329.9M
Bird Audio	22 kHz	4000	Varied	888.3M

**Commands:** The speech command dataset [45] is made up of a series of short audio files with different voices saying a collection of common English words (e.g., “happy” and “five”). From all the data provided [https://github.com/DagsHub/audio-datasets/blob/main/Speech\\_Commands\\_Dataset/README.md](https://github.com/DagsHub/audio-datasets/blob/main/Speech_Commands_Dataset/README.md) we take a random half of the data and exclude any clips that are not 16k long (again for easy saving). We are then left with 47650 series, making a total of  $\sim 750$ M data points.

**Arabic Speech:** This dataset contains 1813 time series of high quality (studio recorded) spoken Arabic utterances sampled at 48kHz – <https://github.com/DagsHub/audio-datasets/tree/main/Arabic-Speech-Corpus>. To reduce the data size without dramatically affecting its quality, we down sample the data by a factor of two (human speech is typically below 24kHz). This gives us a total of  $\sim 300$ M data points.

**Birds:** Finally, we use the bird detection dataset from <https://github.com/DagsHub/audio-datasets/blob/main/Bird-Audio-Detection-challenge/README.md> [46]. This dataset contains a combination of bird and other sounds designed to train machine learning algorithms to detect bird noises. Here we ignore the labels and use the entire dataset in training. Again, to reduce data volumes we down sample by a factor of two, and only use a randomly chosen half of the data. This leaves us with 4000 time series sampled at 22 kHz for a total of  $\sim 900$ M data points.

## B In-Sequence Predictions to Forecasting

Here we simply show an example of how in-sequence test loss correlates with forecasting prediction from roll-out. In particular, in Fig. 4 we show forecasts for three different datasets as a function of model size. Here we use the best weights (i.e., the model that achieved the lowest test loss during training) for each model size and show both in-sequence and forecasting along with the true data. For both the in-sequence and forecasting predictions we show the  $1\sigma$  range of predictions. Although not perfect, it’s clear that as one scales up model size (and therefore in-sequence test loss decreases), forecasting performance also improves substantially. Although we only show three examples here, we observe a similar trend in the forecasting power of our models for a variety of datasets. We leave a more detailed exploration to future work.

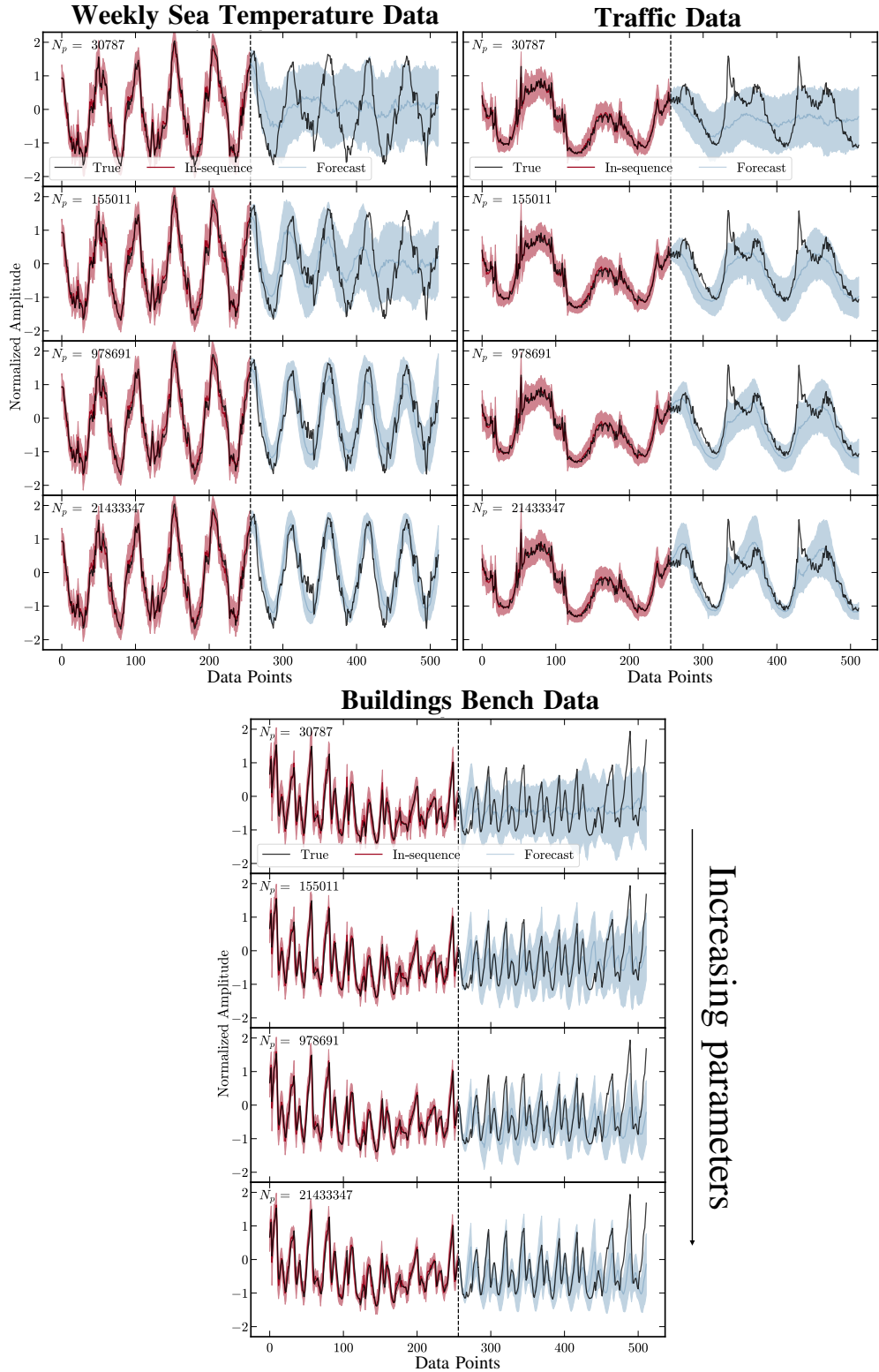


Figure 4: **In-sequence test loss to forecasting:** Here we show the connection between improved in-sequence test loss and forecasting performance as a function of model size. In particular, we show the true data in black with  $1\sigma$  ranges for both in-sequence and forecasting predictions. It is clear that as in-sequence test loss decreases, forecasting also becomes substantially more predictive.